Lattice dynamics of Fe-doped CoO from first principles

2009 J. Phys.: Condens. Matter 21 125601

(http://iopscience.iop.org/0953-8984/21/12/125601)

IOP PUBLISHING JOURNAL OF PHYSICS: CONDENSED MATTER

J. Phys.: Condens. Matter **21** (2009) 125601 (6pp) doi:10.1088/0953-8984/21/12/125601

Lattice dynamics of Fe-doped CoO from first principles

U D Wdowik and K Parlinski

Institute of Technology, Pedagogical University, PL-30-084 Cracow, Podchorazych 2, Poland

E-mail: sfwdowik@cyf-kr.edu.pl

Received 23 October 2008, in final form 9 February 2009
Published 3 March 2009
Online at stacks.iop.org/JPhysCM/21/125601

Abstract

The vibrational dynamics of substitutional Fe and its influence on the vibrational properties of the host CoO matrix have been investigated using *ab initio* calculated Hellmann–Feynman forces. Corrections for the strong on-site interaction have been taken into account via the Hubbard potential U and the local exchange interaction J. Calculations were performed with constant U on Co and variable U on Fe. It was found that Fe impurities exhibit higher values of effective force constant than the original Co. New localized modes are created in the host CoO matrix due to force constant defect between Fe and Co. Iron impurities affect the optical phonon vibrations, while the long wavelength acoustic phonons do not experience changes upon the doping. Mean-squared vibrational amplitudes of cations and anions in the ideal and Fe-doped CoO are compared to the available experimental data. The calculated mean-squared displacements of Fe remain in very good agreement with those measured by Mössbauer spectroscopy.

(Some figures in this article are in colour only in the electronic version)

1. Introduction

Lattice point defects can modify various features of materials. They may affect the vibrational properties of the ideal lattice as well. On the other hand, the changes experienced by the host lattice due to defect incorporation are of rather a local character. Therefore, it is a complicated and difficult task to determine experimentally the local lattice perturbations specific to impurities as well as the dynamical properties of a dopant itself [1, 2].

Ab initio methods offer the possibility of studying the influence of defects on lattice dynamics. Such investigations are still a challenge to a theory of strongly correlated systems. Indeed, for such systems the complicated electronic structure, extensive ionic relaxations, and electronic structure modifications due to impurities remain a demanding task for first-principles calculations. Difficulties also arise from the highly correlated nature of electron interactions, which govern both the electronic structure and the lattice dynamics of the 3d transition-metal oxides [3–5].

Phonon calculations for CoO have been unsuccessful unless one took into account the on-site Coulomb repulsion between 3d electrons [6]. Neglected electron correlations lead to the appearance of unphysical imaginary phonon frequencies. Moreover, Coulomb repulsions that are too small result in artificial soft modes as well.

Typically, in the density-functional theory (DFT), interactions between correlated states are described by the Hubbard potential U and the local exchange interaction J [7–9]. Using appropriate U and J terms, one can properly describe the vibrational properties of a CoO lattice [6].

CoO crystallizes in a rock-salt structure with a lattice constant of 4.2614 Å [10, 11] and it becomes antiferromagnetically ordered below the Néel temperature of about 291 K. Cobalt ions adopt antiferromagnetic ordering of type II (AFII), where planes of spin-up and spin-down sites are stacked in an alternating manner along the [111] direction (see figure 1). The AFII supercell is twice as large as the crystallographic fcc unit cell. The DFT + U approach predicts CoO to be a charge-transfer insulator [12, 13] with an experimental energy gap of about 2.5–2.8 eV [14, 15]. On the other hand, CoO is the non-stoichiometric, cobalt-deficient oxide, which can accommodate a variety of trivalent impurity cations [16, 17]. Several Mössbauer investigations have shown that iron impurities exist in both divalent and trivalent high spin states in CoO (see [18] and references therein).

This paper considers the influence of a substitutional Fe impurity on the lattice dynamics of a charge-transfer insulator,

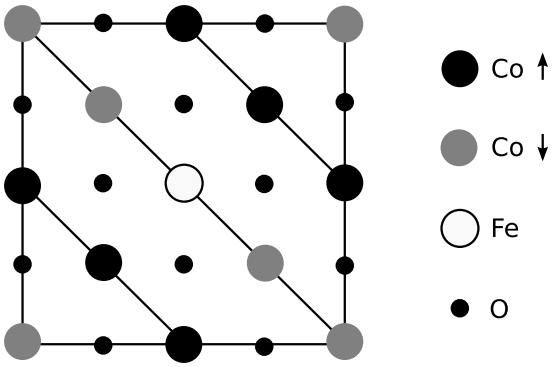

Figure 1. Schematic view of the central layer of the AFII supercell corresponding to the (110) plane of CoO. Large and small circles denote cations and anions, respectively. Spin-up and spin-down cobalt sublattices are shown by black and gray symbols. The iron impurity is marked by an open circle. Slanted lines denote (111) planes.

CoO. Iron is taken as the dopant as to compare our calculations to the existing experiments. One has to note that most of the experimental studies devoted to the lattice dynamics of doped CoO have been performed by Mössbauer spectroscopy which uses ^{57}Fe as a microscopic probe. It is expected that the vibrational dynamics of the Fe-dopant differs from the vibrational dynamics of the cations constituting the ideal CoO lattice. This work attempts to study the lattice dynamics of a real system containing a small amount of magnetic impurities. The present computational study is likely to stimulate further theoretical and experimental investigations in this field of research.

2. Method

A supercell approach was used to model the CoO crystal containing Fe impurities. One has to note that within such an approach the simulation of low defect concentrations is still limited to a few per cent.

The AFII supercell of CoO contains 64 atoms (32 f.u.). One Co atom with fractional coordinates of $(\frac{1}{2}, \frac{1}{2}, \frac{1}{2})$ was replaced by a Fe atom (see figure 1). This leads to an overall concentration of substitutional Fe in CoO of 3.125%. The Fe-doped CoO contains 13 crystallographically non-equivalent atoms. The large size of the supercell separates the periodic defect images by over 8.5 Å, reducing the unphysical interactions between them. Hence, the Fe impurity can be considered as an isolated ion within the Co sublattice.

Calculations were performed using the plane wave basis VASP code [19, 20] which implements the spin-polarized DFT and a projector augmented wave (PAW) technique [21]. The valence electrons of Co, Fe, and O were described by the pseudopotential configurations ($3d^8 4s^1$), ($3d^7 4s^1$), and ($2s^2 2p^4$), respectively. Exchange and correlations were treated within the generalized gradient approximation (GGA). The exchange–correlation functional PW91 [22] was used and plane waves were expanded up to energies of 520 eV. Effects of electron correlation beyond GGA were taken into account within the framework of GGA + U and the simplified (rotationally invariant) approach of Dudarev *et al* [9]. In this approach only the difference $U_{\text{eff}} = U - J$ is meaningful, and hence one can obtain the same results with U_{eff} and $J = 0$. The Coulomb repulsion $U_{\text{Co}} = 7.1$ eV and the local exchange interaction $J = 1$ eV were applied for the Co 3d shell. These values lead to an energy gap for undoped CoO of 2.77 eV [6], which is in good agreement with the experimental energy gap of 2.5–2.8 eV [14]. It should be noted that $U_{\text{Co}} = 7.8$ eV and $J = 0.78$ eV were obtained by Anisimov *et al* [7]. It is worth mentioning that for $U_{\text{Co}} = 7.1$ eV the phonon dispersion curves of CoO reproduce the inelastic neutron scattering data [23] with a reasonable accuracy.

For Fe 3d electrons the Hubbard energy U_{Fe} was varied from 5.1 to 7.1 eV, while $J = 1$ eV was kept constant. These values are representative of those used for the Fe cation in other magnetic insulators [24–27]. The Brillouin zone was sampled using the $2 \times 2 \times 2$ k-point mesh generated by the Monkhorst–Pack scheme. A combination of conjugate gradient energy minimization and quasi-Newton force minimization was used to optimize the geometry and the atomic positions of the initial CoO supercell. The size of the CoO supercell containing the Fe impurity was fixed at the optimized value of the host material and all internal atomic positions were relaxed until the forces were smaller than 10^{-5} eV Å^{-1}. The total energy was converged down to 10^{-7} eV.

The phonon dispersion relations and the vibrational density of states (DOS) for both initial and Fe-doped CoO have been calculated within the harmonic approximation and by using the direct method [28, 29] based on the forces calculated via the Hellmann–Feynman theorem. Each crystallographically independent atom was displaced from its equilibrium position by 0.03 Å in three Cartesian directions. Both positive and negative displacements were applied to minimize the systematic errors. Hence, the total number of calculated displacements was equal to 78. The induced forces acting on all other atoms within the supercell were used to construct the force constant matrix of the system. The phonon frequencies and the corresponding eigenvectors were obtained by diagonalizing the dynamical matrix. The splitting between transverse optic (TO) and longitudinal optic (LO) modes due to the coupling between atomic displacements and a long-range macroscopic electric field was calculated via the introduction of a non-analytical term [30] into the dynamical matrix. The non-analytical contributions takes on the following form [28, 31, 32]:

$$\frac{4\pi e^2}{V\epsilon_\infty \sqrt{M_\mu M_\nu}} \times \frac{[\mathbf{k}\cdot\mathbf{Z}^*(\mu)]_\alpha [\mathbf{k}\cdot\mathbf{Z}^*(\nu)]_\beta}{|\mathbf{k}|^2} \times \exp\{-2\pi i \mathbf{g}\cdot[\mathbf{r}(\mu)-\mathbf{r}(\nu)]\}\frac{1+\cos(\pi|\mathbf{k}|/|\mathbf{k}_{\text{BZ}}|)}{2}, \tag{1}$$

where $\mathbf{k}$ is the wavevector within a Brillouin zone with a center at the reciprocal lattice vector $\mathbf{g}$ and $\mathbf{k}_{\text{BZ}}$ stays for the wavevector parallel to $\mathbf{k}$ having a length from Γ to the Brillouin zone surface. Symbols V, M_μ, and $\mathbf{r}_\mu$ denote the volume of the primitive unit cell, atomic masses, and positions, respectively. The Born effective charge tensors and the high-frequency dielectric constant are denoted by $\mathbf{Z}^*(\mu)$ and ϵ_∞, respectively.

The Born effective charges have been estimated previously for undoped CoO [6] and they amount to $|Z^*| = 2.06$. This value has been used for all ions, while $\epsilon_\infty = 5.3$ has been adopted from [33].

3. Results and discussion

Substitutional Fe remains octahedrally coordinated by the surrounding oxygens and the local lattice relaxations in the vicinity of an impurity lead to a modification of the initial cation–anion distances. Substantial changes are observed for Fe–O bonding; however, they are practically independent on the applied U_{Fe}. The surrounding oxygens are attracted by the Fe impurity. The initial cation–anion distance changes from 2.15 to 2.06 Å while replacing Co by Fe. The Co in the second coordination sphere are displaced outward by 0.03 Å. The rest of the ions in the supercell do not experience significant changes during doping. Hence, the interaction between the impurity and the ions of the host lattice is of a local character.

In the present paper, only the harmonic phonons are considered. A typical approach to the lattice dynamics takes advantage of the periodic symmetry of the crystal, and hence the phonon dispersion relations are given within a primitive unit cell. Solution of the dynamical matrix leads to $3N$ phonon dispersion curves, where N denotes the number of atoms in the primitive unit cell. One has to note that the selection of the primitive unit cell as a crystalline unit is a convention. One can select a larger cell, being a multiplication of the primitive unit cell, and call it a supercell. For such supercell, the dimensions of the dynamical matrix increase to $3N_{\mathrm{S}}$, where N_{S} is the number of atoms in the supercell, the number of phonon dispersion curves increases correspondingly, and the Brillouin zone conjugated with the supercell becomes smaller. An example is the primitive unit cell of CoO containing $N = 2$ atoms and exhibiting six phonon dispersion curves [6]. The $2 \times 2 \times 2$ supercell of CoO with a doubled lattice constant consists of $N = 64$ atoms. The Brillouin zone for such supercell is correspondingly smaller. Therefore, one might expect to have 192 phonon dispersion curves. On the other hand, we know that only six phonon branches exist in the whole reciprocal space. This apparent contradiction is due to the selection of a different kind of unit cell (a supercell) for which the number of phonon dispersion curves is increased.

The above discussion does not take into account the phonon form factor which enters any scattering experiment. The phonon form factor determines whether a given mode is a real/observable mode or is a fake mode (experimentally never seen). The simplest form factor takes on the following form [34, 35]:

$$F^{(p)}(\mathbf{k}, j) = \frac{1}{\mathbf{k}^2} \left| \sum_{\mu} \frac{\mathbf{k} \cdot \mathbf{e}(\mathbf{k}, j; \mu)}{\sqrt{M_\mu}} \right|^2, \tag{2}$$

where M_μ is the mass of the μth atom involved in the j phonon branch at the wavevector $\mathbf{k}$ and $\mathbf{e}(\mathbf{k}, j)$ denotes the polarization vector of the mode $(\mathbf{k}, j)$. The form factor $F^{(p)}(\mathbf{k}, j)$ appears in the dynamical structure factor defining the intensity of one-phonon coherent neutron or x-ray scattering. For all fake modes $F^{(p)}(\mathbf{k}, j) = 0$.

Description of the lattice vibrations within a supercell approach is required for defected systems containing vacancies or impurities, since the point defects lower the original crystal symmetry, making the supercell a primitive unit cell. Due to a partially broken symmetry some fake phonon modes can become visible. Those arisen modes carry information on the defect and the defect's surrounding vibrations. It is known that point defects, even in the harmonic approximation, affect the lattice vibrations, and therefore the appearance of additional modes reflects an influence of the point defect on the host lattice dynamics.

For a general discussion the form factor defined by equation (2) is not always the most convenient, since its value depends upon the crystal orientation with respect to the momentum transfer. A more convenient quantity, called here a *filter*, which indicates the real occupations of the phonon branches, can be obtained by averaging the form factor, equation (2), over all possible relative orientations between $\mathbf{k}$ and $\mathbf{e}(\mathbf{k}, j; \mu)$. This averaging denoted by $\mathrm{d}\Omega$ leads to the following expression [28, 35]:

$$\int_{\Omega} \mathrm{d}\Omega \, F^{(p)}(\mathbf{k}, j) = \tfrac{1}{3} F^{(s)}(\mathbf{k}, j), \tag{3}$$

where $F^{(s)}(\mathbf{k}, j)$ has the following form [28, 35]:

$$F^{(s)}(\mathbf{k}, j) = \left| \sum_{\mu} \frac{\mathbf{e}(\mathbf{k}, j; \mu)}{\sqrt{M_\mu}} \right|^2. \tag{4}$$

Filter $F^{(s)}(\mathbf{k}, j)$ represents the intensity of a given phonon mode and allows one to estimate the relative intensities of all modes across a variety of Brillouin zones. It is able to remove most of the unessential phonon branches carrying very low intensities.

Intensities of the normal modes due to the filter $F^{(s)}(\mathbf{k}, j)$ are shown for the ideal CoO in figure 2. The maximal value of $F^{(s)}(\mathbf{k}, j)$, which corresponds to the highest intensity, was set to 100%. Neutron scattering data [23] measured at 110 K are shown for comparison as well. One has to note that experimental data gather close to the branches carrying intensities higher than 30%. The calculated frequency of the infrared-active mode, ω_{TO}, equals 10.25 THz and the estimated LO–TO splitting amounts to 5.5 THz. The frequency ω_{TO} is very close to the experimentally determined range of TO frequency of 10.40–10.50 THz [23, 33].

The phonon dispersion relations displayed using filter $F^{(s)}(\mathbf{k}, j)$ are shown for Fe-doped CoO in figure 3. The phonon curves are shown for $U_{\mathrm{Fe}} = U_{\mathrm{Co}} = 7.1$ eV. The modes with intensities lower than 5% are not shown. The applied 5% cut-off results in discontinuities observed for some phonon branches. New localized modes are created in the host CoO matrix. Their localization range is confined to the size of the supercell used in the calculations. Localized modes of very diluted impurities are expected to be confined to the vicinity of the impurity. These localized modes are unlikely to be due to the mass defect between Fe and Co as the difference in the respective masses is too small to account for such an effect. Moreover, localized modes appeared

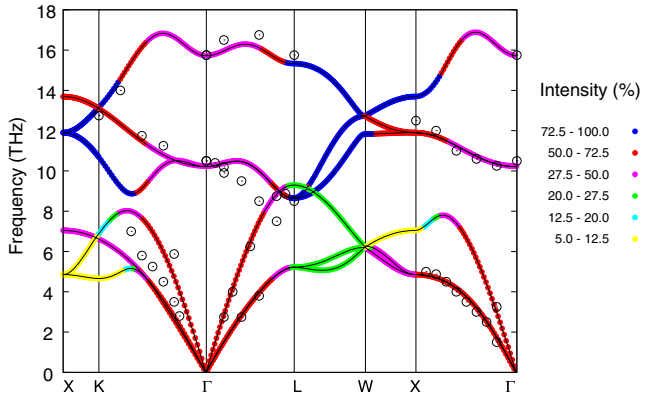

Figure 2. *Ab initio* calculated phonon dispersion relations of CoO (solid line) and dispersion curve intensities (color symbols). The legend gives the linear scale of intensity determined by the filter $F^{(s)}(\mathbf{k}, j)$ for each phonon mode. The mode with the highest intensity is taken as a reference (100%). Experimental data from inelastic neutron scattering [23] are indicated by open symbols.

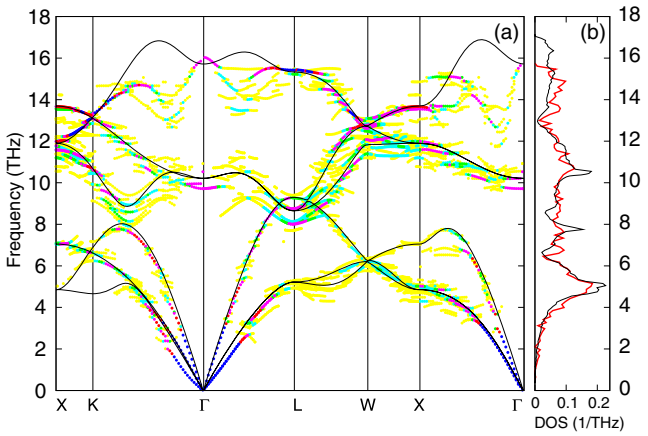

Figure 3. (a) Phonon dispersion relations of Fe-doped CoO shown as intensities defined by the filter (4). Modes with intensities lower than 5% are not shown. Phonons were calculated for $U_{\mathrm{Fe}} = 7.1$ eV. Phonon branches for CoO (solid curve) are shown for comparison as well. The same notation as in figure 1 applies. (b) Phonon DOS for CoO (black curve) and Fe-doped CoO (color curve).

predominantly at higher frequencies, i.e. between 13 and 14.5 THz, which are dominated by the oxygen vibrations. This effect is driven by the change in the force constants at the impurity site. One observes an enhancement of the on-site force constants while replacing Co by Fe. The force constant at the Fe site is dependent upon U_{Fe}. For the applied U_{Fe} of 7.1, 6.1, and 5.1 eV the on-site force constant equals 13.313, 12.783, and 12.264 eV Å^{-2}, respectively. These are higher than the force constant of the host Co in CoO which amounts to 10.013 eV Å^{-2}. The iron impurity introducing locally its own force constants is responsible for the splitting of ω_{TO} into modes corresponding to oxygens vibrating around Co and Fe. This splitting is visible at the Γ-point in figure 3. One estimates ω_{TO} using the modes with intensities higher than 50% and finds TO vibrations of oxygens surrounding Co to be slightly higher than the respective vibrations of oxygens surrounding Fe. Again, the TO frequencies of oxygens located in the Fe neighborhood depend slightly upon U_{Fe}. They equal 9.72, 9.68, and 9.67 THz for the applied U_{Fe} of 7.1, 6.1, and 5.1 eV, respectively. The frequency ω_{TO} of oxygens close to Co remains practically constant versus U_{Fe} and amounts to 10.51 THz. It is slightly higher than the theoretical ω_{TO} obtained for the ideal CoO (10.25 THz); however, it still lies in the experimental range (10.40–10.50 THz).

The main contribution to the high-frequency acoustic phonons comes from the Co sublattice, while the high-frequency optic phonons are dominated by the dynamics of the light oxygen ions [6]. For Fe-doped CoO the acoustic branches remain sharp and they are very close to the acoustic branches of the ideal CoO lattice, provided the small wavevectors are considered. Both transverse and longitudinal acoustic modes experience some smearing while approaching the Brillouin zone boundaries, i.e. at larger wavevectors.

Information on the defect and the defect's surrounding vibrations can be also obtained from the partial phonon

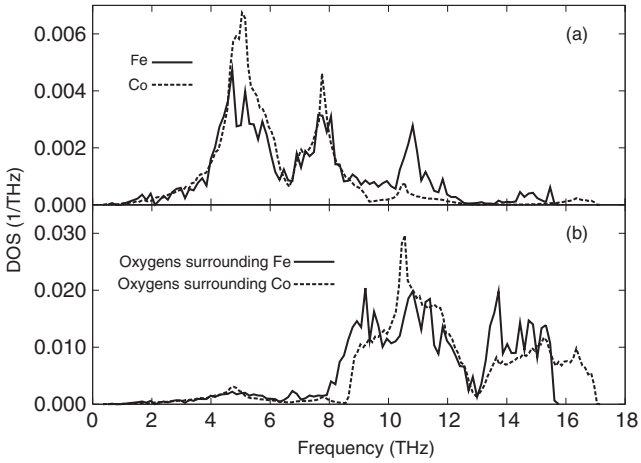

Figure 4. (a) Partial phonon DOS for Co in undoped CoO (dashed line) and for Fe in doped CoO (solid line). (b) Partial DOS for oxygens neighboring Co in undoped CoO (dashed line) and Fe in doped CoO (solid line). Calculations are done for $U_{\mathrm{Fe}} = 7.1$ eV. Partial phonon densities of states are defined by equation (5).

densities of states defined in the following way [28, 34, 35]:

$$g_{i,\mu}(\omega) = \frac{1}{nd\Delta\omega} \sum_{\mathbf{k},j} |e_i(\mathbf{k}, j; \mu)|^2 \, \delta_{\Delta\omega}(\omega - \omega(\mathbf{k}, j)), \quad (5)$$

where $e_i(\mathbf{k}, j; \mu)$ is the ith Cartesian component of the eigenvector of the mode $(\mathbf{k}, j)$ for the atom μ, $\Delta\omega$ denotes the frequency interval, n is the number of sampling wavevector points, d stands for the dimension of $\mathbf{D}(\mathbf{k})$, while $\delta_{\Delta\omega}(x)$ equals 1 if $|x| \leqslant \Delta/2$, otherwise it is equal to zero. The total phonon density of states results from the summation $g(\omega) = \sum_{i,\mu} g_{i,\mu}(\omega)$.

The phonon DOS for the Fe impurity is compared to the phonon DOS of host Co in figure 4(a). It can be seen that the low-frequency phonons of Fe and the host Co are similar to each other. At higher frequencies the Fe

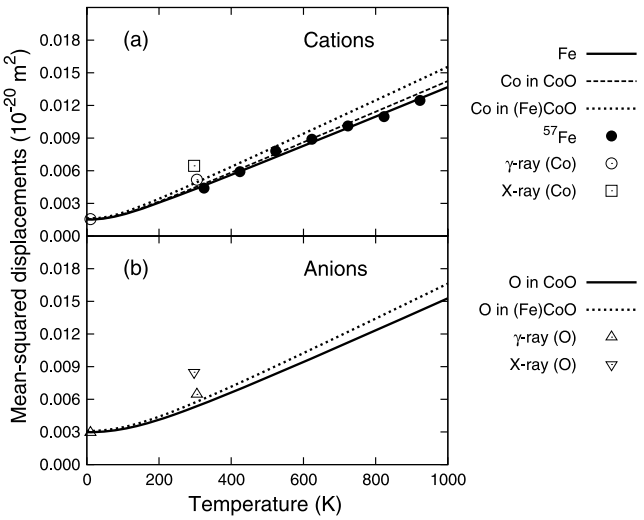

Figure 5. (a) Mean-squared displacements versus temperature for cations in undoped and Fe-doped CoO. Solid, dashed, and dotted curves correspond to Fe impurity, Co in CoO, and Co in Fe-doped CoO, respectively. (b) Mean-squared displacements versus temperature for anions in undoped and Fe-doped CoO. Solid and dotted curves are for O in CoO and O in Fe-doped CoO, respectively. Calculations are done for $U_{\mathrm{Fe}} = 7.1$ eV. The γ-ray data [11] are shown as open circles and up-triangles for Co and O, respectively. X-ray data [36] are denoted by open squares and down-triangles for cations and anions, respectively. Solid symbols indicate Mössbauer data of substitutional ^{57}Fe in the host CoO matrix [18].

DOS peaks are enhanced compared to Co peaks. The Fe impurity modifies vibrations of its local surrounding, and hence essential differences in the partial DOS are found for those oxygens which are the defect nearest-neighbors. Figure 4(b) compares the partial DOS of oxygens surrounding Fe to the partial DOS of those oxygens which surround Co in undoped CoO. The high-frequency spectrum of Fe surrounding oxygens seems to be slightly shifted against the spectrum of Co surrounding oxygens.

The intensity of the radiation scattered by the crystal contains a Debye–Waller factor defined as $\exp\{-W_\mu(\mathbf{k})\}$, where

$$W_\mu(\mathbf{k}) = \tfrac{1}{2}(2\pi\mathbf{k}\cdot\mathbf{B}(\mu)\cdot(2\pi\mathbf{k}))\,. \tag{6}$$

$\mathbf{B}(\mu)$ represents the static correlation function of the μth atom displacement, $U(\mu)$, from its equilibrium position. $\mathbf{B}(\mu)$ is a second-rank symmetric tensor having the following components:

$$B_{ij}(\mu) = \langle U_i(\mu)U_j(\mu)\rangle\,. \tag{7}$$

$\mathbf{B}(\mu)$ represents the mean-squared displacement (MSD) of the atom μ and it is expressed by the diagonal and off-diagonal partial phonon density of states $g_{il,\mu}(\omega)$ taking on the following form [28, 34, 35]:

$$B_{il}(\mu) = \frac{\hbar r}{2M_\mu}\int_0^\infty \mathrm{d}\omega\, g_{il,\mu}(\omega)\,\omega^{-1}\coth\left(\frac{\hbar\omega}{2k_{\mathrm{B}}T}\right), \tag{8}$$

where $\hbar$ is the Planck constant, k_{B} denotes the Boltzmann constant, and T is the temperature. Symbols M_μ and r denote the mass of the atom μ and the number of degrees of freedom in the primitive unit cell, respectively.

Table 1. Theoretical and experimental MSD at 10 K [11] and the MSD slopes at elevated temperatures for Co, O, and Fe in doped and undoped CoO. MSD is given in (Å^2 $\times$ 10^{-2}), while its slope is given in (Å^2 $\times$ 10^{-5} K^{-1}).

	Fe-doped CoO				
U_{Fe} (eV)	7.1	6.1	5.1	CoO	Exp. [11]
Fe	0.152	0.156	0.160		
Co	0.163	0.163	0.163	0.157	0.148(3)
O	0.309	0.310	0.311	0.298	0.291(30)
MSD slopes at elevated temperatures					
Fe	1.337	1.402	1.514		
Co	1.527	1.538	1.560	1.395	
O	1.561	1.581	1.611	1.425	

Figure 5 shows the mean-squared amplitude of atomic vibrations versus temperature calculated for $U_{\mathrm{Fe}} = 7.1$ eV. The average MSD is shown for Co and oxygens in Fe-doped CoO. Calculations are compared to MSD obtained from γ-ray [11], x-ray [36], and Mössbauer experiments [18]. The temperature range is limited to 1000 K to avoid contributions from anharmonicity. In the entire temperature range, cations have lower vibrational amplitudes than anions, reflecting the difference in their masses. Theoretical and experimental MSD of cations and anions in doped and undoped CoO are collected in table 1. The changes of MSD with increasing temperature are also given in table 1 by the respective MSD slopes calculated for temperatures exceeding 300 K. The MSD of Fe increases with the decreasing U_{Fe} due to the decreased effective force constant at the Fe site. A similar effect is encountered for Co and O in Fe-doped CoO. For $U_{\mathrm{Fe}} = U_{\mathrm{Co}} = 7.1$ eV, Fe shows smaller MSD than Co constituting either undoped or doped CoO. At low temperatures the difference between MSD of Fe and Co in doped CoO reaches about 7%, while at elevated temperatures it is nearly two times greater. This difference becomes smaller when lowering U_{Fe}. The MSD slope of Fe obtained with $U_{\mathrm{Fe}} = 7.1$ eV agrees very well with the MSD slope of nucleogenic ^{57}Fe measured by emission Mössbauer spectroscopy [18]. Since its MSD is smaller than the MSD of Co in the undoped CoO, hence the Debye temperature (Θ_{D}) of CoO estimated using the dynamics of Fe impurity results in the lower $\Theta_{\mathrm{D}} = 440$ K [18] compared to $\Theta_{\mathrm{D}} = 500$ K calculated for the ideal CoO lattice.

4. Summary and conclusions

A supercell approach was used to model the structure of CoO crystal containing a Fe impurity. The lattice dynamics of doped CoO has been studied within a harmonic approximation and by using a direct method. A filter which enables one to analyze numerous phonon dispersion curves was applied. This allowed the phonon dispersion relations to be presented closer to the dispersion curves of a real defected sample.

It was shown that the vibrational properties of a Fe impurity in the CoO crystal can be essentially different from the vibrational properties of the host cations. Differences in the vibrational dynamics of the dopant and host atoms arise

from the difference in their force constants. The Fe impurity modifies the vibrations of the oxygens in its neighborhood and introduces new localized modes into the CoO matrix. Therefore, the use of ^{57}Fe as a probe in a crystal studied by emission Mössbauer spectroscopy could provide modified magnitudes of the measured quantities with respect to the appropriate values for the ideal crystal.

Acknowledgments

This work was supported by the Polish Ministry of Scientific Research (MNiSW), grant no. 3T11F 031 29. The Interdisciplinary Modeling Center (ICM), Warsaw University, Poland is acknowledged for providing the computer facilities under the grant no. G28-12.

References

[1] Horton G K and Maradudin A A (ed) 1975 *Dynamical Properties of Solids* vol 2 (Amsterdam: North-Holland)
[2] Dederichs P H and Zeller R 1980 Dynamical properties of point defects in metals *Point Defects in Metals II* (*Springer Tracts in Modern Physics* vol 87) (Berlin: Springer)
[3] Savrasov S Y and Kotliar G 2003 *Phys. Rev. Lett.* **90** 056401
[4] Dudarev S L, Peng L M, Savrasov S Y and Zuo J M 2000 *Phys. Rev.* B **61** 2506
[5] Massidda S, Posternak M, Baldereschi A and Resta R 1999 *Phys. Rev. Lett.* **82** 430
[6] Wdowik U D and Parlinski K 2007 *Phys. Rev.* B **75** 104306
[7] Anisimov V I, Zaanen J and Andersen O K 1991 *Phys. Rev.* B **44** 943
[8] Anisimov V I, Solovyev I V, Korotin M A, Czyzyk M T and Sawatzky G A 1993 *Phys. Rev.* B **48** 16929
[9] Dudarev S L, Botton G A, Savrasov S Y, Humphreys C J and Sutton A P 1999 *Phys. Rev.* B **57** 1505
[10] Jauch W, Reehuis M, Bleif H J and Kubanek F 2001 *Phys. Rev.* B **64** 052102
[11] Jauch W and Reehuis M 2002 *Phys. Rev.* B **65** 125111
[12] Sawatzky G A and Allen J W 1984 *Phys. Rev. Lett.* **53** 2339
[13] Zaanen J, Sawatzky G A and Allen J W 1985 *Phys. Rev. Lett.* **55** 418
[14] van Elp J, Wieland J L, Eskes H, Kuiper P, Sawatzky G A, de Grot F M F and Turner T S 1991 *Phys. Rev.* B **44** 6090
[15] Powell R J and Spicer W E 1970 *Phys. Rev.* B **2** 2182
[16] Grimes R W and Chen S P 2000 *J. Phys. Chem. Solids* **61** 1263
[17] Wdowik U D and Parlinski K 2008 *Phys. Rev.* B **77** 115110
[18] Ruebenbauer K and Wdowik U D 2004 *J. Phys. Chem. Solids* **65** 1785
[19] Kresse G and Furthműller J 1999 *Computer Code VASP* Vienna, Austria
[20] Kresse G and Furthműller J 1996 *Phys. Rev.* B **54** 11169
[21] Kresse G and Joubert J 1999 *Phys. Rev.* B **59** 1758
[22] Perdew J P, Chevary J A, Vosko S H, Jackson K A, Pederson M R, Singh D J and Fiolhais C 1992 *Phys. Rev.* B **46** 6671
[23] Sakurai J, Buyers W J L, Cowley R A and Dolling G 1968 *Phys. Rev.* **167** 510
[24] Mazin I I and Anisimov V I 1997 *Phys. Rev.* B **55** 12822
[25] Kuneŝ J, Rosner H, Kasinathan D, Rodriguez C O and Pickett W C 2003 *Phys. Rev.* B **68** 115101
[26] Tran F, Blaha P, Schwarz K and Novák P *Phys. Rev.* B **74** 155108
[27] Mosey N J, Liao P and Carter E A 2008 *J. Chem. Phys.* **129** 014103
[28] Parlinski K 2008 *Software PHONON* Cracow, Poland
[29] Parlinski K, Li Z Q and Kawazoe Y 1997 *Phys. Rev. Lett.* **78** 4063
[30] Pick R M, Cohen M H and Martin R M 1970 *Phys. Rev.* B **1** 910
[31] Parlinski K and Kawazoe Y 1999 *Phys. Rev.* B **60** 15511
[32] Parlinski K, Li Z Q and Kawazoe Y 2000 *Phys. Rev.* B **61** 272
[33] Gielisse P J, Plendl J N, Mansur L C, Marshall R, Mitra S S, Mikolajewicz R and Smakula A 1965 *J. Appl. Phys.* **36** 2446
[34] Sjőlander A 1958 *Ark. Fys.* **14** 315
[35] Wdowik U D and Parlinski K 2008 *Phys. Rev.* B **78** 224114
[36] Sasaki S, Fujino F and Takeuchi Y 1979 *Proc. Japan. Acad. Ser.* B **55** 43